Available online at www.sciencedirect.com
ScienceDirect
Journal of Colloid and Interface Science 317 (2008) 493–500
JOURNAL OF Colloid and Interface Science
www.elsevier.com/locate/jcis

Synthesis of alcoholic ZnO nanocolloids in the presence of piperidine organic base: Nucleation-growth evidence of $Zn_5(OH)_8Ac_2{\cdot}2H_2O$ fine particles and ZnO nanocrystals

F. Grasset [a,b,*], O. Lavastre [c,*], C. Baudet [c], T. Sasaki [b], H. Haneda [d]

[a] *Université de Rennes 1, "Science Chimiques de Rennes" UMR UR1-CNRS 6226, Groupe Chimie du Solide et Matériaux, Campus de Beaulieu, CS74205, F-35042 Rennes cedex, France*
[b] *International Center for Young Scientists, National Institute for Materials Science, Namiki 1-1, Tsukuba, Ibaraki 305-0044, Japan*
[c] *Université de Rennes 1, "Science Chimiques de Rennes" UMR UR1-CNRS 6226, Groupe Catalyse et Organométalliques, Campus de Beaulieu, CS74205, F-35042 Rennes cedex, France*
[d] *National Institute for Materials Science, Namiki 1-1, Tsukuba, Ibaraki 305-0044, Japan*

Received 25 June 2007; accepted 22 September 2007

Available online 2 October 2007

Abstract

Piperidine as a new free OH^- organic base has been successfully used to prepare $Zn_5(OH)_8(Ac)_2{\cdot}2H_2O$ particles (named Zn-HDS) or concentrated alcoholic ZnO sols. Considering the applications of Zn-HDS and ZnO compounds, as well as interests of these synthesis mechanisms for fundamental chemistry, such investigations are of importance. This strategy not only allows preparing Zn-HDS compounds at room temperature but also brings evidence of some new nucleation-growth, and permits the preparation of well crystalline ZnO nanocrystals at low temperature (maximum 60 °C). It was possible to convincingly prove that the formation of Zn-HDS phase is concomitant to the ZnO nanocrystals formation and that Zn-HDS could be considered as an intermediate initiator of ZnO nanocrystals. A parallel approach was used for the fast screening of the synthesis progress.

Keywords: Zinc oxide; Nanocolloids; Zn-HDS; Nucleation; Growth; Piperidine; Parallel screening

1. Introduction

Zinc oxide (ZnO), a wide band gap (3.37 eV) semiconductor with large exciton binding energy, has been used in a wide range of applications such ultra-violet (UV) light emitters, spin functional devices, gas sensors, transparent electronics, surface acoustic wave devices [1] and as a well-known catalyst [2]. Various chemical, electrochemical or physical deposition methods have been used to prepare functional ZnO materials. Our strategy to design new materials is based on the sol–gel chemical synthesis of functional ZnO nanocolloids in alcohol [3–5]. Nevertheless, although this "bottom-up" approach has been known for more than 20 years [6–8], recently, some works have pointed out that zinc based colloidal sols obtained from the sol–gel route derived from the Spanhel and Anderson method were not pure zinc oxide [9,10]. The isolated powders from colloidal sols are a mixture of nanometer sized ZnO, zinc acetate (Ac) and acetate derivative zinc hydroxide double salt $Zn_5(OH)_8Ac_2{\cdot}2H_2O$ (so called Zn-HDS). Moreover, the nucleation-growth process proposed by Spanhel et al., via the ethanol media route, is based on the hydrolysis and condensation of $Zn_4O(Ac)_6$, $Zn_{10}O_4(Ac)_6$ clusters using a fractal construction concept [11,12]. If, Tokumoto et al. proved without doubt that after 3 h reflux of ethanol–zinc acetate mixture, the precursors synthesized is well $Zn_4O(Ac)_6$ tetrameric clusters [11], the possible precursors of ZnO nanocrystals have been reported to be $Zn_4O(Ac)_6$, $Zn_{10}O_4(Ac)_6$ or Zn-HDS in the presence of acetate ions in "basic" alcoholic solution [9,11–14]

* Corresponding author. Faxes: +33 2 23 23 67 99, +33 2 23 23 69 39.
E-mail addresses: grasset@univ-rennes1.fr (F. Grasset), olivier.lavastre@univ-rennes1.fr (O. Lavastre).

0021-9797/$ – see front matter
doi:10.1016/j.jcis.2007.09.078

(the autoprotolysis constant of ethanol is $10^{-19.1}$, so ethanol is neutral at pH 9.6). What implies that the discussion about the hydrolysis-condensation reaction process of the ZnO nanocrystals is always very active [10,12–17]. In particular, the interesting question about the fact that the formation of Zn-HDS phase is concomitant to the ZnO formation or arises from the reaction of ZnO with zinc acetate during ageing of the colloidal sol [10,12,14,17]. In this way, considering the various applications of ZnO or Zn-HDS as well as continued interests in these synthesis mechanisms for fundamental chemistry, further investigations are of importance.

In this communication, we address a complete study of the chemical reactions to prepare ZnO nanocolloid using free OH^- organic base "piperidine" and to use parallel approach in order to screen new "basic" route, which enables to bring some nucleation-growth evidence.

2. Experimental

2.1. Processing of precursor solution

The ethanol–zinc precursors solution was prepared using similar route as published by Spanhel and Anderson [5]. Briefly, 0.06 mol (13.17 g) of $Zn(Ac)_2{\cdot}2H_2O$ (from Fluka) were suspended in 0.6 L of ethanol (from Fluka or Wako) under ambient atmosphere and distilled during ∼180 min in a preheated (80 °C) silicon oil bath of a rotary evaporator. At the end of this procedure, 0.25 L of condensate and 0.35 L of hygroscopic reaction mixture were obtained. Subsequently, 0.25 L of cold ethanol was quickly added to the hygroscopic mixture in order to obtain 0.1 M precursor solution. The obtained transparent solution was stored at 4 °C.

2.2. Screening of different bases and ratio base/Zn using parallel approach

2.2.1. Primary screening

4 solutions (2 M in methanol) were prepared with the bases **1** to **4**. These stock solutions were diluted to give 7 others solutions at 1, 0.4, 0.2, 0.1, 0.05, 0.025 and 0.020 M, respectively. 300 μL of these 32 bases solutions were added in 1 mL vials according to Table 1. 300 μL of the Zn precursor solution 0.1 M were added, and then the vials were closed and shacked by hand. The ratio Base/Zn varies from 20/1 to 1/5 as indicated in Table 1. After 30 min, 50 μL aliquots of each vial were transferred to a 96 well-plate for parallel UV–vis spectroscopic analysis. The UV–vis measurement was performed with a plate reader BioTeck Instrument INC (model μQuant) to qualitatively detect the presence or the absence of a strong absorbance at 325 nm (notes X in Table 1) after blank subtraction. TMAOH was used as reference for this primary screening.

2.2.2. Secondary screening

The same protocol as previously described was used starting from 1 M solutions of bases **4** to **7** in methanol. After addition of the Zn precursor solution to the different diluted solutions at 1, 0.45, 0.4, 0.36, 0.31, 0.28, 0.24, 0.2 M, the final ratio base/Zn varies from 10/1 to 2/1 as indicated in Table 2. The same qualitative UV–vis spectroscopic evaluation as the primary screening was performed. LiOH was used as reference for this secondary screening.

Table 1
Qualitative evaluation of bases **1** to **4** with different ratio base/Zn for the synthesis of ZnO nanocolloids

Base/Z	*n*			
	1	**2**	**3**	**4**
20/1	X		X	X
10/1	X		X	X
4/1	X		X	X
2/1	X		X	X
1/1				
1/2				
1/4				
1/5				

Note. X: Presence of strong absorbance at 325 nm after blank subtraction. Bases: **1**—KOH, **2**—$CsCO_3$, **3**—TMAOH, **4**—piperidine.

Table 2
Qualitative evaluation of bases **4** to **7** with different ratio base/Zn for the synthesis of ZnO nanocolloids

Base/Z	*n*			
	4	**5**	**6**	**7**
10/1	X		X	
4,4/1	X		X	
4/1	X		X	
3,6/1	X		X	
3,2/1	X		X	
2,8/1	X		X	
2,4/1	X		X	
2/1	X		X	

Note. X: Presence of strong absorbance at 325 nm after blank subtraction. Bases: **4**—piperidine, **5**—pyridine, **6**—LiOH, **7**—bipyridine.

2.3. Processing of ZnO nanocolloids

At 20 °C and under magnetic stirring, 20 mL of a methanolic piperidine solution (0.36 M) were rapidly added to 20 mL of the ethanolic precursor solution, yielding turbid solution in less than one hour. By keeping this turbid solution at 20 °C under magnetic stirring, a very "milky" solution is observed during 2 months. In a parallel experiment, by increasing the temperature of the turbid solution, it is transformed into a clear nanocolloid after 2 days and after few minutes at 31 and 60 °C, respectively. After cooling and ageing at room temperature, these colloids remained transparent and stable for periods of up to a few weeks. By mixing the methanolic piperidine solution and the precursor solution at 4 °C and keeping the mixture at 4 °C, there is a precipitate after 2 h with no apparition of clear colloid even after 2 months. In order to precipitate nanopowder from clear nanocolloids: (i) heptane or cyclohexane was used as organic nonsolvents using the process described in Ref. [9]; (ii) the supernatant was removed by centrifugation (5000 rpm/10 min). In the case of "milky" colloids, only centrifugation was used to remove supernatant. In some cases, the precipitate was washed with acetone and dried at room temperature.

2.4. UV–vis and luminescence

UV–vis spectra of the colloids and films were recorded with a Varian CARY 5 spectrometer. The emission spectra were measured with a JASCO FP-6500 spectrophotometer. Measurements were performed using a quartz cell having a path length of 10 mm. The intensity of emitted light was detected at a right angle to the incident light and an excitation wavelength of 290 nm was used. The photoluminescence spectra were recorded at room temperature, after dilution in ethanol.

2.5. X-ray intensity measurements

X-ray diffraction data were recorded at room temperature on a Rigaku using the Bragg–Brentano geometry with Cu$K\alpha$ radiation (40 kV, 40 mA, integration time range from 2 to 10 s) and a secondary monochromator. The average apparent crystallite size (ε_β) was estimated from a whole diffraction pattern profile analysis, using last developments implemented in the Fullprof.2k program (Version July 2006-LLB, Juan Rodriguez-Carvajal). By description of instrumental and intrinsic profiles by normalized Voigt function (convolution of Gaussian and Lorentzian functions), size and strain effects can be separated from the whole profile analysis based on the different angular dependence of the Gaussian and Lorentzian full-width-at-half-maximum (H_G and H_L, respectively), according to the following equations:

$$H_G^2 = \left(U_{\text{strain\_iso}} + (1-\xi)\,D^2_{\text{strain\_aniso}}\right)\text{tg}^2\,\theta + \frac{G_{\text{size\_iso}}}{\cos^2\theta},$$

$$H_L = \left(X_{\text{strain\_iso}} + \xi\,D_{\text{strain\_aniso}}\right)\text{tg}\,\theta + \frac{Y_{\text{size\_iso}} + F_{\text{size\_aniso}}}{\cos\theta},$$

where U, X, ξ, G and Y are refinable parameters, and D and F are analytical functions (which depend on a set of additional refinable parameters) to model the *hkl*-dependent broadening due to strain and size effects, respectively. "Perfect" Y_2O_3 powder was used as a standard to determine the instrumental resolution function (IRF) of the diffractometer. The observed line broadening was modeled by isotropic size effects, leading to $1/\cos\theta$ dependent terms of H_G and H_L (Y and G parameters in Fullprof, respectively) contribution to the size effects. Refinement of $\text{tg}\,\theta$ dependent isotropic strain parameters (U and X parameter in Fullprof) did not improve significantly the profile fitting. For each diffraction pattern, a counter zero point and the unit-cell parameters were refined in addition to the Y and G parameters. The background level was defined by a polynomial function.

2.6. Morphological investigations by SEM and TEM

SEM photographs by Jeol JSM 6301F were taken to examine the shape and size of the nanocrystals. Samples for SEM were simply prepared by depositing precipitated and dried powders directly on aluminum metal sample holder. HRTEM images were taken with JEOL JEM 2100F equipped with CCD camera, EDX analysis and HAADF-STEM mode. Samples for TEM analysis were prepared by placing a drop of the diluted solution in mesh copper grids, allowing the solvent in the grid to evaporate at room temperature.

3. Results and discussion

As stated in the introduction section, the synthesis of ZnO nanocolloids using refluxing alcoholic zinc acetate solution has been a popular approach since last 20 years, for which it is impossible to give an exhaustive list of references. Moreover, although nucleation and growth of ZnO nanocrystals using alcoholic zinc acetate solution have been recently studied carefully [10–17], it is always under debate. Nevertheless, concerning the reaction products obtained after reflux of ethanolic zinc acetate solution, three papers are recommended reading of special interest [11–13]. Briefly, Tokumoto et al. have proved that the structure of the precursor produced by refluxing ethanolic zinc acetate solution is an oligomeric acetate-capped clusters of formula $[Zn_4O(Ac)_6]$ [13], which can be generated by condensation $[Zn_{10}O_4(Ac)_{12}]$ as proposed by Spanhel et al. [11,12]. The structural similarity of these clusters with ZnO let easily imagine the further condensation of this molecular units into ZnO [11–13,18] nanocrystals but nothing is completely proved.

We have studied the role played by different bases **1–7** (Tables 1 and 2) to a refluxing ethanolic zinc acetate solution on the synthesis of ZnO nanocolloids at room temperature. Firstly, combinatorial chemistry experiments were used to screen the hopeful base. The experimental conditions for synthesis of ZnO nanocolloids influence directly their formation and their size, and consequently their physical properties [12]. To vary at the same time the nature of the studied bases and the base/Zn ratio for each base requires a significant number of experiments. This is a time and materials consuming process. In addition, if all these experiments proceed sequentially over a certain period (1 to 2 weeks) there is a risk of evolution of the solutions of precursors and thus a risk of bad reproducibility. Recently, several examples involving combinatorial methods were reported for material science or catalysis [19–21]. Also we worked out a miniaturized parallel approach allowing simultaneous screenings of several experimental conditions starting from the same solutions of precursors.

The primary screening led us to test simultaneously 4 different bases and 8 different ratio base/Zn. These 32 conditions (see Table 1) were tested with 300 μL of different solutions of bases and precursors of Zn. Their evaluation by parallel UV spectroscopy led us to detect, by the intense absorption at 325 nm, the best conditions able to generate nanocrystals of ZnO. The "traditional" bases **1** and **3** were actually detected by this approach in parallel. This validates the present method even if it uses very small amounts of chemical substances. No interesting result was obtained with cesium carbonate, indicating that, for inorganic bases, OH^- is better than other anions. On the other hand, an unexpected result was obtained with piperidine **4**. This led us to test other organic amines by using LiOH like reference (Table 2). The expected results with LiOH were indeed detected, again validating the miniaturized parallel approach. On the other hand, none of two organic bases **5** and **7** (pyridine fam-

ily) generated the same results than the secondary amine piperidine. We thus showed that the miniaturized parallel approach could reproduce results (KOH, LiOH, TMAOH) obtained until now with large volumes and amount of substances, and on the other hand could simultaneously test a large number of experiments to detect a new way for synthesis of ZnO nanocrystals. It is important to note that it was difficult to predict the specificity of piperidine at the beginning of this study even if piperidine, in contrary to pyridine compounds, is a strong alkylamine base ($pK_a = 11.3$ at 20 °C) and can be considered as a good proton acceptor: $NHR_2 + HOH \leftrightarrow NH_2R_2^+ + OH^-$.

3.1. Characterization of concomitant formation of Zn-HDs and ZnO nanocrystals

Regarding the combinatorial chemistry results, the second part of this work focused on the synthesis of concentrated ZnO nanocolloids using piperidine (noted Pip) as free OH^- organic base with ratio Pip/Zn = 0.36. We report in Figs. 1 and 2 the optical densities of solution (after dilution in ethanol), as a function of time and temperature. For the optical density as a function of time, the temperature of the solution was kept at 31 °C. For the optical density as a function of the temperature, the measurements of the optical density was performed after the same mixture solution was kept for 30 min at 35, 45, 55 and 60 °C, respectively (for the same solution, full time is 2 h to reach 60 °C). All these spectra show the band gap of ZnO nanocrystals, with a blue shift with respect to the bulk oxide, due to quantum confinement [12,15]. The effect of ageing on the absorption characteristics of ZnO nanocolloids is shown in Figs. 1 and 2. In all the cases, a red shift in the onset of absorption was observed with increasing time. The 2 days ageing sols at 31 °C or the 30 min ageing sol at 60 °C give a classical UV–vis absorption spectrum without scattering, whereas the other solutions show a broad spectrum relative to scattering of large particles according to Lord Rayleigh theory. These data are in good agreement with the manually observed turbidity of the solution (Fig. 1) and with study of the hydrodynamic diameter by dynamic light scattering (see supporting information). The hydrodynamic diameter observed for the turbid solution is larger than 1.5 μm, whereas it is only about 13 nm for clear ageing colloids. The data reported in Figs. 1 and 2 confirm the disappearance of the turbidity after 2 days at 31 °C or after increasing temperature at 60 °C. We should note that the formation of macroscopic particles early in solution has also been previously observed by Haase et al. [22] in the preparation of ZnO sols in methanol with excess Zn^{2+}. They have noted that the precipitate obtained disappeared after only 5 min. Similar results were also observed in our recent work [3,4], with large turbidity appeared following the addition of TMAOH base into still hot propanolic zinc solution but vanished after 2 or 3 min. Contrary to these observations, using LiOH or TMAOH base into cold ethanolic zinc acetate solution does not bring about turbidity and seems to agree with the fractal construction concept [12]. In order to characterize the large particles, organic solvent as heptane or cyclohexane was added to the turbid solution. The X-ray diffraction study of this low temperature and

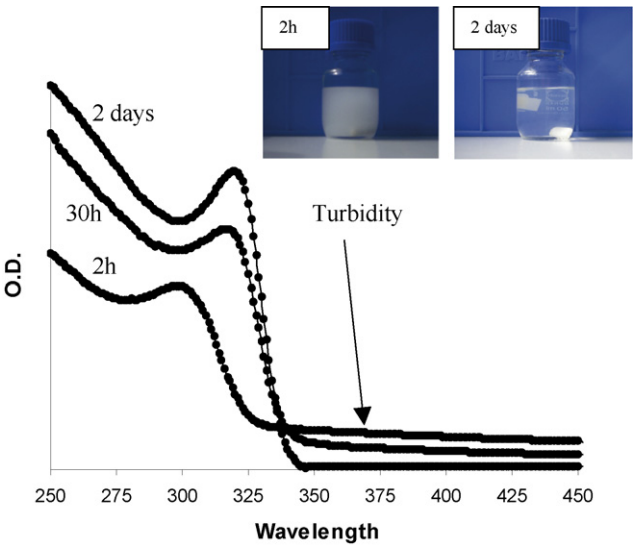

Fig. 1. UV–vis absorption spectra of ZnO nanocrystals as function of time keeping at 31 °C.

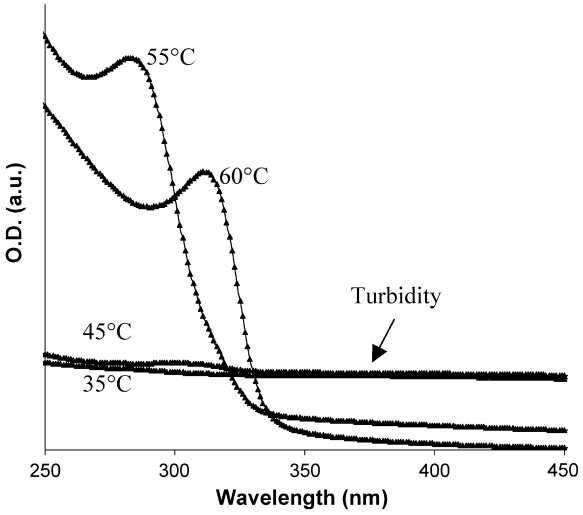

Fig. 2. UV–vis absorption spectra of ZnO nanocrystals as function of temperature. The solution has been kept during 30 min at 35, 45, 55 and 60 °C, respectively.

short ageing time intermediate compounds is shown in Fig. 3. XRD pattern suggested that the obtained compound belongs to the wide family of layered double hydroxides with the well-known $Zn_5(OH)_8(Ac)_2{\cdot}2H_2O$ (zinc hydroxide double salt so called Zn-HDS). Hydroxyl double salts (HDS), with the general formula $[M^{II}_{1-x}Me^{II}_{1+x}(OH)_{3(1-y)}]^+X^{n-}_{z(1+3y)/n}{\cdot}zH_2O$ (M and Me correspond to divalent metals, X represents anions), deserve a lot of attention owing to their potential applications in anion-exchange materials [23]. Although, the peak labeled (001) corresponds to the interlayer distance of typical Zn-HDS (14.6 Å) is comparable to the respective literature [23–26], we cannot completely rule out the structural role-played by piperidine in the formation of Zn-HDS [27]. The broadening of harmonic reflection demonstrated the very small number of layers along the *c* axis. Moreover, broad and asymmetrically shaped peaks are observed at higher angles, a result of turbostratic effect [24]. It

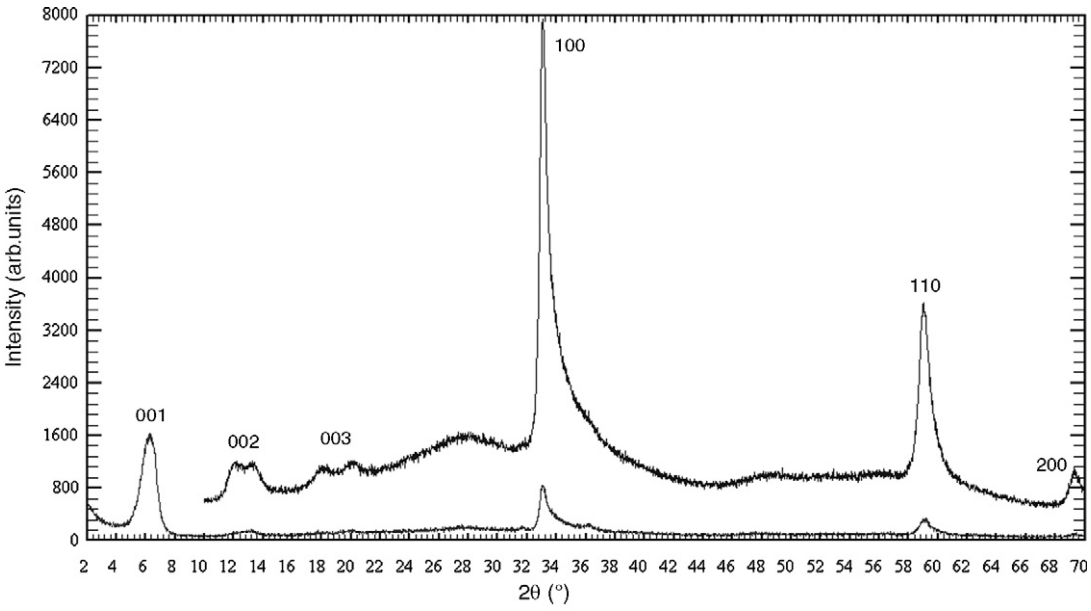

Fig. 3. XRD pattern of Zn-HDS compound. The upper pattern is a zoom of the lower part. Miller *hkl* indices for selected peaks are given.

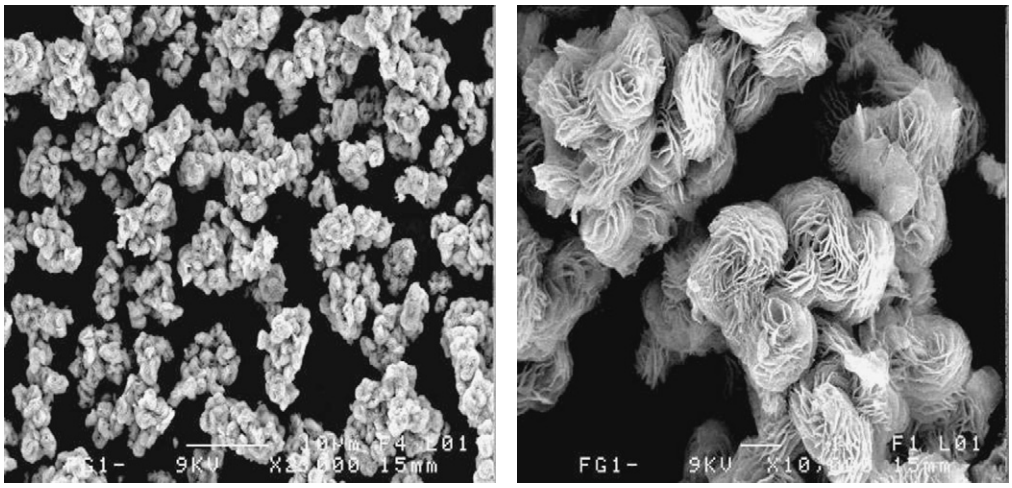

(a) (b)

Fig. 4. SEM images of the Zn-HDS powder obtained after 1 day and adding of cyclohexane.

should be noted that a broad peak around 26–30° in the pattern is due to a glass sample holder for the XRD measurement. The SEM (Fig. 4) reveals porous and narrow micron sized particles with self-assembly "flower" morphology as observed recently by Fujihara et al. during the fabrication of porous ZnO films by a pyrolytic transformation of Zn-HDS [26]. Dark field STEM images (Fig. 5) of these micron-sized particles have proved the highly disordered lamellar compound, and agree with XRD, DLS and SEM data. We should note that Zn-HDS is observed by TEM even in the absence of precipitation by organic solvent and we assumed that the turbidity is due to scattering of large Zn-HDS particles. Nevertheless, on the same mesh copper grid, a careful STEM and HRTEM experiments reveal the presence of crystallized ZnO nanocrystals concomitantly to Zn-HDS formation. In Fig. 5 (inset) the lattice spacing values of the observed nanodomains was calculated to be 0.26 nm identical to (002) interplanar distance of ZnO, which are $d_{002} = 0.260$. Since the discovery of quantum size effect in ZnO, the conventional optical spectroscopy became a popular method to study the fluorescence spectra of growing ZnO nanocolloids [6–9,12, 28–31]. In addition to HRTEM experiments, the presence of primary ZnO nanocrystals during the early stage of hydrolysis at room temperature was proved by photoluminescence measurements.

Fig. 6 shows the photoluminescence spectra recorded just after mixing methanolic piperidine solution and the precursor solution during 130 min. Indeed, the well-known intense and broad emission band situated in the visible part of the spectrum is observed [6–9,12,28–31] (to be directly observed by human eyes at room temperature, see supporting information). We can easily observe the red shift of the visible trap luminescence (Fig. 6). The lower part of Fig. 6 represents the contour

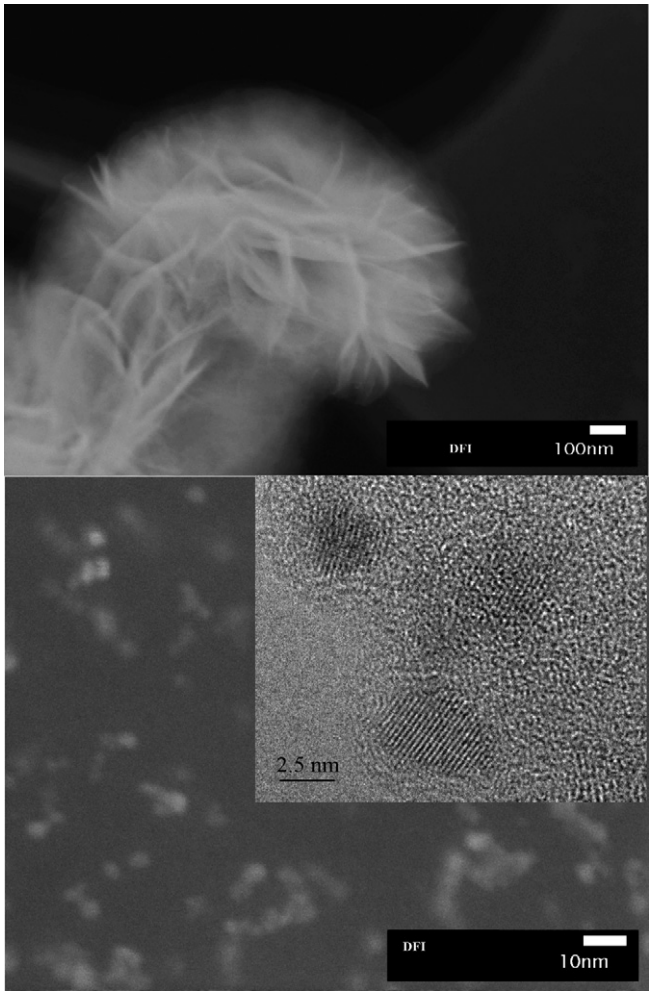

Fig. 5. Dark field STEM and HRTEM images of the Zn-HDS microparticles (upper) and ZnO nanocrystals (lower) by drop directly on the mesh copper grid from diluted colloids (ageing 3 h).

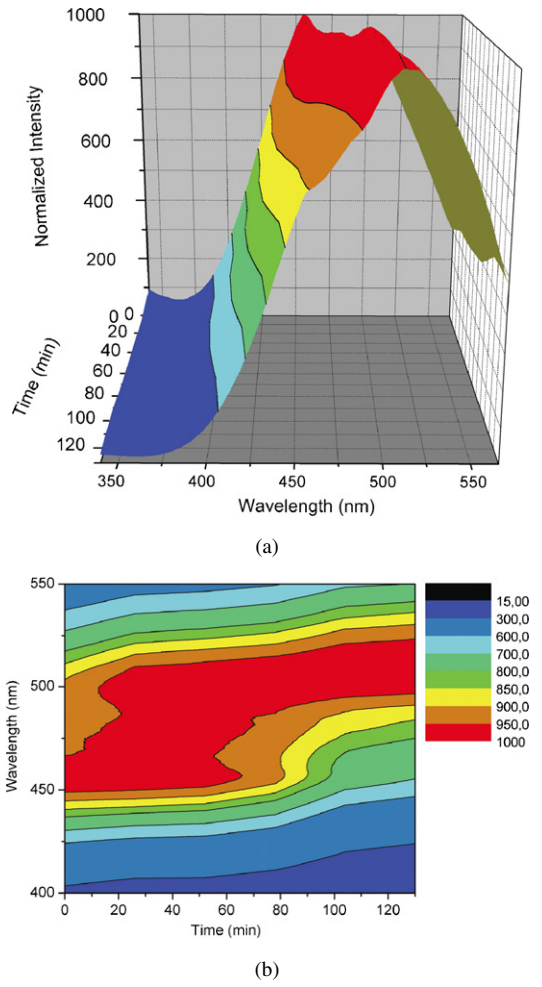

Fig. 6. (a) Emission spectra of ZnO nanocolloids during first 130 min ageing. (b) Contour map in the wavelength and time plane. The solutions were excited with a light of a wavelength of 290 nm.

map in the wavelength and time plane. This indicates the presence of ZnO nanocrystals with size below 6 nm [12] and clearly the growth of ZnO nanocrystals during the early stage of hydrolysis at room temperature, concomitantly to the formation of Zn-HDS nanocrystals.

3.2. Dissolution of Zn-HDS

The present work not only proved by numerous techniques the simultaneous formation of Zn-HDS and ZnO nanocrystals but also seem to provide evidence that Zn-HDS could be transformed into ZnO nanocrystals at low temperature. Indeed, after ageing the colloids at least at 31 °C, the turbidity vanished and a clear solution was obtained as proved by optical (Fig. 1) and DLS measurements (see supporting information). Fig. 7 shows the observed XRD patterns of a single phase ZnO nanopowder (according to accuracy of XRD method) obtained from all transparent prepared sols. The nanopowders could be obtained by adding heptane or cyclohexane into the sols, which generates a rapid phase separation of a precipitate, and by centrifugation at 5000 rpm during 10 min. In all the cases, no peak from Zn-HDS was observed at $2\theta = 6°$. The noise signal at low theta is due to the Bragg–Brentano configuration. We should note that even in the case of the "milky" sol ageing at room temperature for more than 2 months, only ZnO phase was observed from the precipitate obtained only by centrifugation (heptane or cyclohexane was not used in that case). The diffraction peaks are broad and the average apparent crystallite size (ε_β) of the particles was estimated to be 3.6 nm, which was confirmed by TEM experiment (Fig. 8). Observed aggregated nanocrystals could be unambiguously attributed to hexagonal wurtzite structure. The HRTEM spacing values of the [001] zone axis correspond to the distance of ZnO ($d_{100} = 0.28$ nm) (Fiche ICDD JCPDS N° 361451). Regarding our results, we propose like Hosono et al. [14,26] that $Zn_5(OH)_8(Ac)_2{\cdot}2H_2O$ could be considered, even in basic media, as an important intermediate product following this chemical equation: $Zn_5(OH)_8(Ac)_2{\cdot}2H_2O \rightarrow 2HAc + 5ZnO + 5\ H_2O$.

4. Conclusion

Using a parallel approach, it was easy to find new base candidates for low temperature synthesis of ZnO nanocrystals in order to prepare stable and highly concentrated ZnO nanocol-

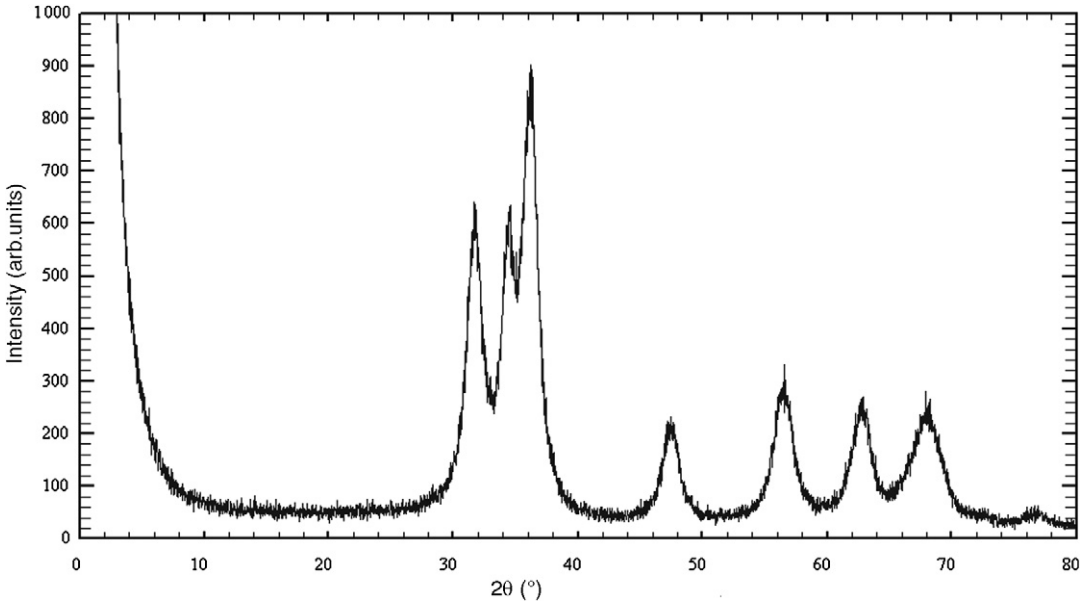

Fig. 7. X-ray powder diffraction profiles of typical ZnO nanopowders obtained from flocculated sol.

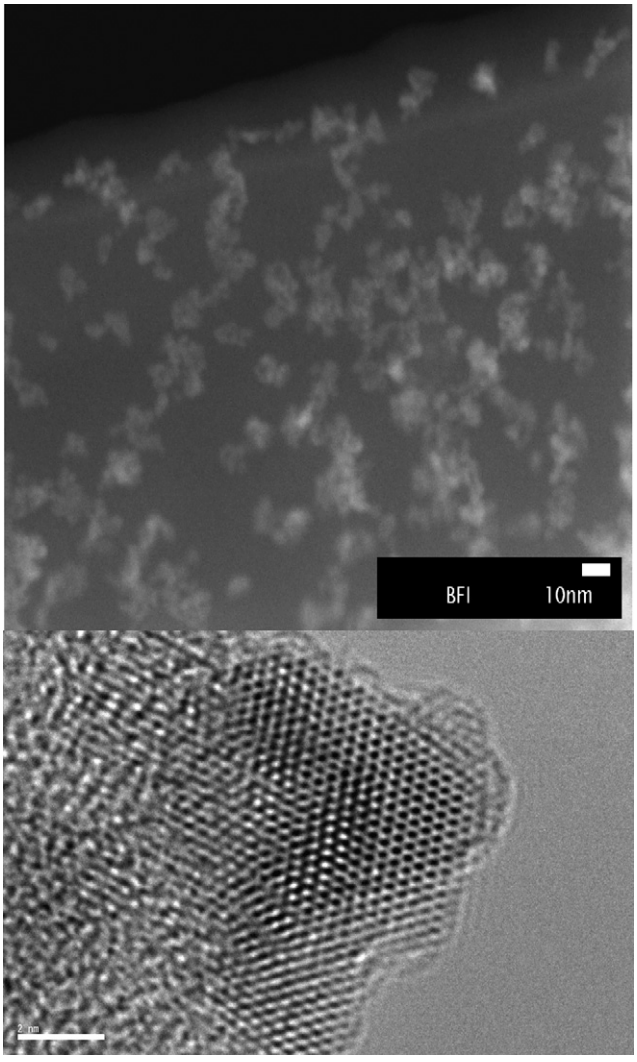

Fig. 8. Dark field STEM (upper) and HRTEM (lower) images of ZnO aggregated nanocrystals. (HRTEM: The scale bar corresponds to 2 nm.)

loids. Thanks to the slow chemical reaction, we found that by using piperidine as a base, Zn-HDs can be synthesized at room temperature and some interesting improvements on nucleation-growth can be proposed. We assumed that when turbidity is observed, it should imply that Zn-HDS appears to be the main initiator of ZnO nanocrystal. But with due respect to other chemical routes, we propose a competition process during the growth of ZnO nanocrystals with a fractal construction concept depending of the base used and the media. It is effortless to understand that the hydrolysis-condensation reaction process of the ZnO nanocrystals could not be simple and that it results from a competition between various mechanisms. Such specific behavior may be of particular interest to fundamental chemistry as well as in applications such as for Zn-HDS in anion-exchange materials. Finally, this novel, room-temperature and low-cost generation of ZnO nanocrystals from Zn-HDS enriches the known range on zinc based colloidal sols and sheds light on the potential application of ZnO nanomaterials for their promising and tailored optical properties.

Acknowledgments

This work was financially supported by CITRennes, NIMS/ICYS, the University of Rennes 1, CNRS and C'Nano North-Ouest Network. The authors thank J. Le Lannic for supplying the SEM images. Fabien Grasset thanks cordially Professor Y. Bando, Director of International Center for Young Scientist (ICYS).

Supporting information

The online version of this article contains additional supporting information.

Please visit DOI: 10.1016/j.jcis.2007.09.078.

References

[1] S.J. Pearton, D.P. Norton, K. Ip, Y.W. Heo, T. Steiner, Prog. Mater. Sci. 50 (2005) 293.
[2] J. Liqiang, Q. Yichun, W. Baiqi, L. Shudan, J. Baojiang, Y. Libin, F. Wei, F. Honggang, S. Jiazhong, Sol. Energy Mater. Sol. Cells 90 (12) (2006) 1773.
[3] F. Grasset, G. Starukh, L. Spanhel, S. Ababou-Girard, D. Su, A. Klein, Adv. Mater. 17 (3) (2005) 294.
[4] F. Grasset, L. Spanhel, S. Ababou-Girard, Superlat. Microstruct. 38 (4–6) (2005) 300.
[5] F. Grasset, S. Cordier, Y. Molard, C. Perrin, M. Guilloux-Viry, S. Pechev, N. Saito, H. Ryoken, T. Sasaki, H. Haneda, Int. J. Nanotech. 1–2 (2008), in press.
[6] U. Koch, A. Fojtik, H. Weller, A. Henglein, Chem. Phys. Lett. 122 (1985) 507.
[7] D.W. Bahnemann, C. Kormann, M.R. Hoffmann, J. Phys. Chem. 91 (1987) 3789.
[8] L. Spanhel, M.A. Anderson, J. Am. Chem. Soc. 113 (1991) 2826.
[9] E.A. Meulenkamp, J. Phys. Chem. B 102 (1998) 5566.
[10] M.S. Tokumoto, S.H. Pulcinelli, C.V. Santilli, V. Briois, J. Phys. Chem. B 107 (2003) 568.
[11] T. Schmidt, G. Müller, L. Spanhel, Chem. Mater. 10 (1998) 65.
[12] L. Spanhel, J. Sol–Gel Sci. Technol. 39 (2006) 7.
[13] M.S. Tokumoto, V. Briois, C.V. Santilli, S.H. Pulcinelli, J. Sol–Gel Sci. Technol. 26 (2003) 547.
[14] E. Hosono, S. Fujihara, T. Kimura, H. Imai, J. Sol–Gel Sci. Technol. 29 (2004) 71.
[15] Wood, M. Giersig, M. Hilgendorff, A. Vilas-Campos, L.M. Liz-Marzán, P. Mulvaney, Aust. J. Chem. 56 (2003) 1051.
[16] Z. Hu, G. Oskam, P.C. Searson, J. Colloid Interface Sci. 263 (2003) 454.
[17] V. Brois, C. Giorgetti, E. Dartyge, F. Baudelet, M.S. Tokumoto, S.H. Pulcinelli, C.V. Santilli, J. Sol–Gel Sci. Technol. 39 (2006) 25.
[18] R. Bertoncello, M. Bettinelli, M. Casarin, A. Gulino, E. Tondello, A. Vittadini, Inorg. Chem. 31 (1992) 1558.
[19] O. Lavastre, I. Illitchev, P.H. Dixneuf, G. Jegou, T. Oboyet, J. Am. Chem. Soc. 124 (2002) 5278.
[20] O. Lavastre, J. Morken, Angew. Chem. Int. Ed. Engl. 38 (21) (1999) 3163.
[21] O. Lavastre, N. Pinault, Z. Mincheva, in: Principles and Methods for Accelerated Catalyst Design, in: NATO Sciences Series ASI, Kluwer Academic, Dordrecht, 2001, pp. 135–151.
[22] M. Haase, H. Weller, A. Henglein, J. Phys. Chem. 92 (1988) 482.
[23] R.Q. Song, A.W. Xu, B. Deng, Q. Li, G.Y. Chen, Adv. Funct. Mater. 17 (2007) 296.
[24] L. Poul, N. Jouini, F. Fievet, Chem. Mater. 12 (2000) 3123.
[25] E. Kandare, J.M. Hossenlopp, J. Phys. Chem. B 109 (2005) 8469.
[26] E. Hosono, S. Fujihara, T. Kimura, H. Imai, J. Colloid Interface Sci. 272 (2004) 391.
[27] X.M. Chen, Y.X. Jong, Th.C.W. Mak, Inorg. Chem. 33 (1994) 4586.
[28] R.D. Yang, S. Tripathy, Y. Li, H.-J. Sue, Chem. Phys. Let. 411 (2005) 150.
[29] A. Van Diken, E.A. Meulekamp, D. Vanmaekelbergh, A. Meijerink, J. Lumin. 87 (2000) 454.
[30] S. Sakohara, M. Ishida, M.A. Anderson, J. Phys. Chem. B 102 (1998) 10169.
[31] M.L. Kahn, T. Cardinal, B. Bousquet, M. Monge, V. Jubera, B. Chaudret, ChemPhysChem. 7 (2006) 2392.